CrystEngComm

ROYAL SOCIETY OF CHEMISTRY

PAPER

View Article Online
View Journal | View Issue

Cite this: *CrystEngComm*, 2022, **24**, 4440

On the energetic stability of halogen bonds involving metals: implications in crystal engineering†

Ismael Benito, Rosa M. Gomila and Antonio Frontera *

Received 19th April 2022,
Accepted 4th May 2022

DOI: 10.1039/d2ce00545j

rsc.li/crystengcomm

This work reports a combined computational and experimental analysis of the ability of square planar d^8 transition metal complexes to establish unconventional halogen bonding interactions with chloro-, bromo-, and iodopentafluorobenzene as σ-hole donors. Typical M···Ha (M = transition metal and Ha = halogen) interactions are coordination bonds (frequently halides acting as counter ions) or semicoordination bonds (neutral lone pair donor halogens). However, in recent times a new binding mode has been described in the literature with a reverse donor–acceptor role. That is, directional C–Br,I···M halogen bonding (HaB) interactions have been reported where the metal center acts as the electron-rich atom and the halogen atom acts as the acceptor *via* its σ-hole. In addition to the Cambridge Structural Database (CSD) survey of exemplifying X-ray structures, this manuscript reports a DFT study that investigates the relative ability of Ni, Pd, and Pt square planar complexes to participate in HaBs with chloro-, bromo-, and iodopentafluorobenzene.

Introduction

Progress in crystal engineering, a term coined by G. Desiraju, has allowed the generation of deep knowledge on noncovalent interactions and their influence on crystal packing.[1] A relevant consequence is the highly productive design and synthesis of multicomponent crystals with tailored physicochemical properties.[2] In the last decade, σ-hole interactions have become active players in this field.[3] That is, elements belonging to groups 14–17 of the periodic table frequently act as Lewis acids establishing directional interactions with a variety of Lewis bases, π-systems, and anions.[4] These interactions are termed tetrel,[5] pnictogen,[6] chalcogen,[7] and halogen bonds[8] for elements belonging to groups 14, 15, 16 and 17, respectively.

After hydrogen bonding,[9] halogen bonding (HaB) is the most popular σ-hole interaction.[10,11] Actually, this interaction has inspired and motivated the generalization of the σ-hole concept to groups 14–16.[12] HaBs involving the heavier halogen atoms (bromine and iodine) are nowadays commonly used in crystal engineering,[13] catalysis,[14] biological supramolecular chemistry,[15] molecular recognition of anions,[16] and membrane transport.[17]

The most used electron donors in HaB-based crystal engineering are lone pair bearing atoms, such as N, O, and halogen atoms.[8] Moreover, HaB assemblies involving π-systems as donors have also been reported[18] and several theoretical works[19] have analysed and compared Ha···π and lp–π interactions that can be formed depending on the relative orientation of the halogen atom (σ-hole or negative belt pointing to the π-system). Recently, unconventional HaBs have been described, where the electron donor is a transition d^8 metal and the occupied d_{z^2}[M] orbital acts as a σ-hole acceptor instead of more conventional Lewis bases (see Scheme 1).[20,21] This type of interaction is counterintuitive and often unnoticed by the original authors, since positively charged metals are usually recognized as electron acceptors. The nucleophilicity of the d_{z^2}[M] orbital can be modulated by the presence of nucleophiles (other d^8 metals or electron donors) located at the opposite side of the σ-hole donor.[22]

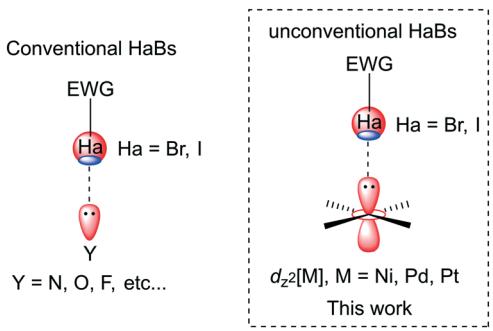

Scheme 1 Conventional (LP as electron donors) and unconventional (metal as electron donors) HaBs. EWG: electron withdrawing group.

Departament de Química, Universitat de les Illes Balears, Crta. de Valldemossa km 7.5, 07122 Palma, Spain. E-mail: toni.frontera@uib.es

† Electronic supplementary information (ESI) available: X-ray coordinates of the optimized complexes. See DOI: https://doi.org/10.1039/d2ce00545j

In this manuscript, a combined CSD analysis and theoretical study is reported to investigate the ability of divalent metals of group-10 of the periodic table to participate in halogen bonding complexes. For the theoretical DFT study (PBE0-D3/def2-TZVP level of theory), three σ-hole donors (halopentafluorobenzenes) and three acceptors were used, as detailed in Scheme 2. The three square planar metal complexes used in this work are neutral. Two 3-oxoprop-1-en-1-olate anions were used as organic ligands. It should be mentioned that, along with experimental studies, metal-involving HaBs were previously studied theoretically using single-point DFT calculations.[23,24]

Computational methods

The calculations of the non-covalent interactions were carried out using Gaussian-16 (ref. 25) and the PBE0-D3/def2-TZVP level of theory.[26,27] For the heavier elements Pd, I, and Pt, this basis set implements ECPs and relativistic effects.[27,28] The complexes were fully optimized using the C_{2v} symmetry constraint. The interaction energies were computed by calculating the difference between the energies of isolated monomers (optimized geometries) and their assembly. Bader's "Atoms in molecules" theory (QTAIM)[29] analysis was performed by means of the Multiwfn program.[30] The molecular electrostatic potential surfaces were computed using the Gaussian-16 software.[25]

In order to assess the nature of the interactions in terms of being attractive or repulsive and reveal them in real space, the NCIplot index was used, which is a method for plotting non-covalent interaction regions[31] based on a visualization index that is derived from the electronic density.[32] The reduced density gradient (RDG), which came from the density and its first derivative, was plotted as a function of the density (mapped as isosurfaces) over the molecule of interest. The sign of the second Hessian eigenvalue times the electron density [*i.e.*, $\mathrm{sign}(\lambda_2)\rho$ in atomic units] enabled the identification of attractive/stabilizing (blue-green coloured isosurfaces) or repulsive (yellow-red coloured isosurfaces) interactions using 3D-plots. The NCIplot index parameters used in this work were: RGD = 0.5; $\rho_{\text{cut-off}}$ = 0.04 a.u.; colour range: −0.04 a.u. ≤ $\mathrm{sign}(\lambda_2)\rho$ ≤ 0.04 a.u. The QTAIM/NCIplot figures were presented using VMD software.[33] The NBO calculations were performed using the NBO 7.0 version[34] at the same level of theory. The donor–acceptor NBOs were presented using the VMD software.[33]

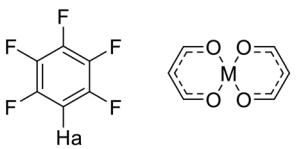

1, Ha = Cl
2, Ha = Br
3, Ha = I

4, M = Ni
5, M = Pd
6, M = Pt

Scheme 2 Halogen bond donors (left) and acceptors (right) used in this work.

Results and discussion

CSD examples exhibiting Br,I···M HaB contacts

In this section, several X-ray structures and co-crystals containing square planar Ni(II), Pd(II), and Pt(II) complexes are highlighted. First of all, it should be mentioned that in this work, instead of using the stringent Bondi's[35] van der Waals (vdW) radii for groups 10 and 17, those proposed by Batsanov were used,[36a] which are gathered in Table 1. Although Bondi's vdW radii are the most used criterion to designate a noncovalent contact,[35] the values for group-10 metals seem largely underestimated, as suggested by several investigations.[36] For instance, Hu *et al.*[36b] proposed 1.97 Å, Batsanov proposed 2.00 Å, and Alvarez[36c] even proposed 2.40 Å as reliable values for the vdW radius of Ni(II), whilst Bondi's vdW radius for this atom is only 1.63 Å. Batsanov's value was selected herein because it is more restrictive than Alvarez's value and almost identical to Hu's proposal.[36b]

Fig. 1 shows two selected X-ray structures involving Ni(II) as the electron donor and bromine (refcode **PUGRIU**)[38] or iodine (refcode **VAPVAK**)[39] as Lewis acids (σ-hole donors). The halogen bond distances are significantly shorter than $\sum R_{\text{vdW}}$ (3.90 Å for Ni + Br and 4.10 Å for Ni + I) and longer than the sum of covalent radii ($\sum R_{\text{cov}}$ = 2.44 Å for Ni + Br and 2.63 Å for N + I), thus supporting the existence and noncovalent nature of the Ni···Ha contacts. The interactions are less directional than the conventional HaBs, with C–Ha···Ni angles of 152° for Br and 162° for I.

For Pd(II), two structures were selected (see Fig. 2), which form homodimers in the solid state where the C–Br bond is pointing to the middle of the Ni–O coordination bond in **RECTEZ**[40] and the Ni–Br coordination bond in **REYJAH**.[41] Therefore, in both structures, bifurcated HaBs are formed. The Br···Ni distances are shorter than $\sum R_{\text{vdW}}$ and longer than $\sum R_{\text{cov}}$, thus disclosing the noncovalent nature of the contacts.

An additional X-ray structure is highlighted in Fig. 3a (refcode **RAPQOQ**).[42] It is a bi-palladium(II) complex with bridging 3,4-dibromo-2,5-dioxo-2,5-dihydropyrrol-1-ide ligands. Remarkably, this molecule self-assembles in the solid state creating dimers governed by the formation of two symmetrically equivalent Br···Pd interactions. The combined

Table 1 Covalent (cov) and Batsanov's van der Waals (vdW) radii of elements of groups 10 and 17 in Å

Period	G-10[a] (cov)	G-10 (vdW)	G-17[a] (cov)	G-17 (vdW)
3		—	1.02 (Cl)	1.80 (Cl)
4	1.24 (Ni)	2.00 (Ni)	1.20 (Br)	1.90 (Br)
5	1.39 (Pd)	2.05 (Pd)	1.39 (I)	2.10 (I)
6	1.36 (Pt)	2.05 (Pt)		—

[a] From ref. 37.

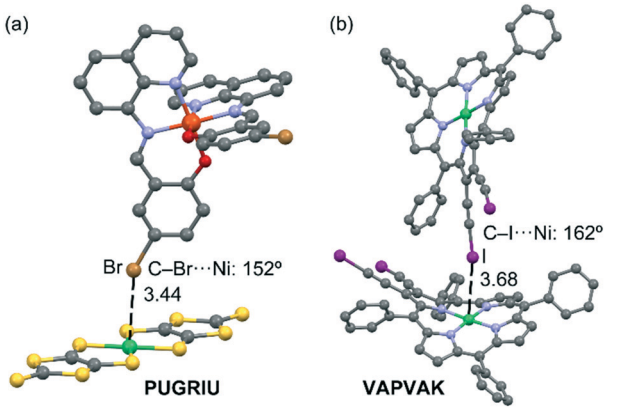

Fig. 1 X-ray structures of CSD reference codes **PUGRIU** (a) and **VAPVAK** (b). Distances are in Å. H-atoms were omitted for clarity.

QTAIM/NCIplot presentation shown in Fig. 3b further corroborates the formation of HaBs that are characterized by a bond critical point (CP, small red sphere) and a bond path (orange line) connecting the Br atom to the Pd(II) metal center. No other bond CP and path connects the Br-atom to the $PdCN_2O$ nucleophilic core. The self-assembled dimer is further stabilized by two symmetric CH···Br H-bonds characterized by a bond CP and a bond path connecting the negative belt of the Br atom to one aromatic H-atom. Both interactions are also characterized by green reduced density gradient (RDG) NCIplot isosurfaces, thus revealing the attractive nature of both interactions.

For Pt(II), an iodoform solvate (refcode **UKAWOU**)[43] and a cocrystal (refcode **ROZNUS**)[44] were selected to illustrate the HaBs. As was also observed in the structures above Ni(II) and Pd(II), the directionality of the contacts was around 160° and the distances were shorter than $\sum R_{vdW}$ and longer than $\sum R_{cov}$, thus suggesting the noncovalent nature of the contacts. As further commented on below (MEP calculations), the σ-hole at iodine is quite extended, ensuring that it is acting as an electron acceptor in the I···Pt(II) contacts.

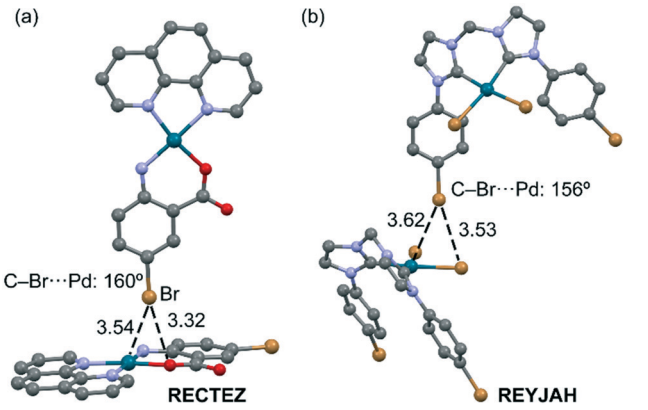

Fig. 2 X-ray structures of CSD reference codes **RECTEZ** (a) and **REYJAH** (b). Distances are in Å. H-atoms were omitted for clarity.

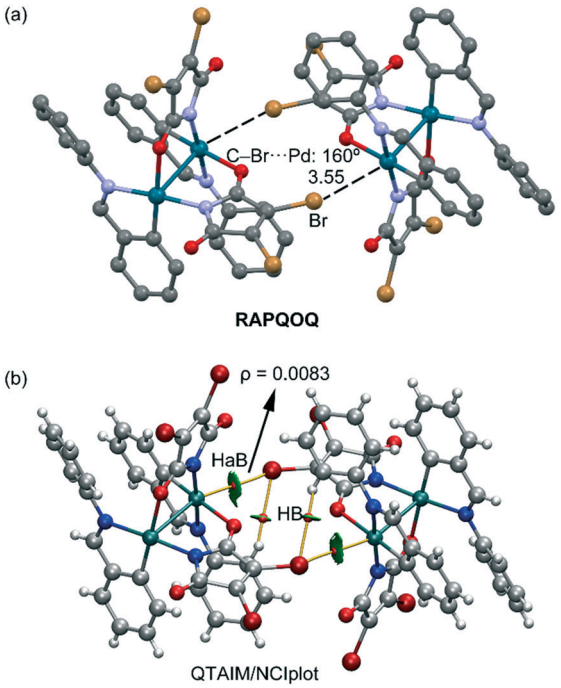

Fig. 3 (a) X-ray structures of CSD reference code **RAPQOQ**. The distance is in Å. H-atoms were omitted for clarity. (b) Combined QTAIM/NCIplot analysis of **RAPQOQ** with indication of the HaB and HB contacts. The density at the bond CP is given in a.u.

More interesting is the **UHEGAR** structure[45] (see Fig. 5) that forms self-assembled dimers in the solid state, establishing two symmetric Br···Pt HaBs. It can be observed in Fig. 5a that the Br···Pt distance is quite short (3.39 Å) and the C–Br···Pt(II) angle is 161°, in line with the rest of the structures shown in Fig. 1–4. Remarkably, the combined QTAIM/NCIplot analysis shown in Fig. 5b not only confirms the existence of the HaB contacts (bond CPs connecting the Br and Pt atoms) but also that this self-assembled dimer is held together exclusively by the formation of these unconventional HaBs.

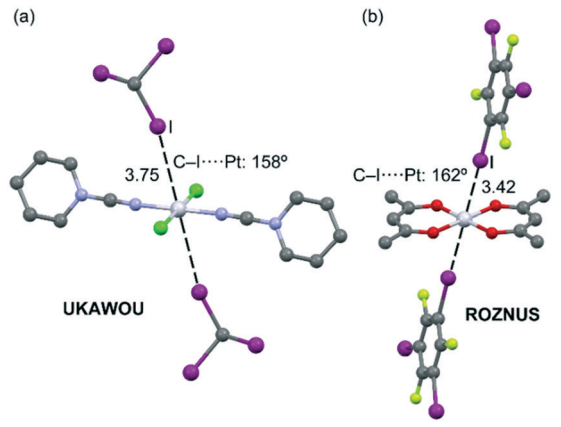

Fig. 4 X-ray structures of CSD reference codes **UKAKOU** (a) and **ROZNUS** (b). Distances are in Å. H-atoms were omitted for clarity.

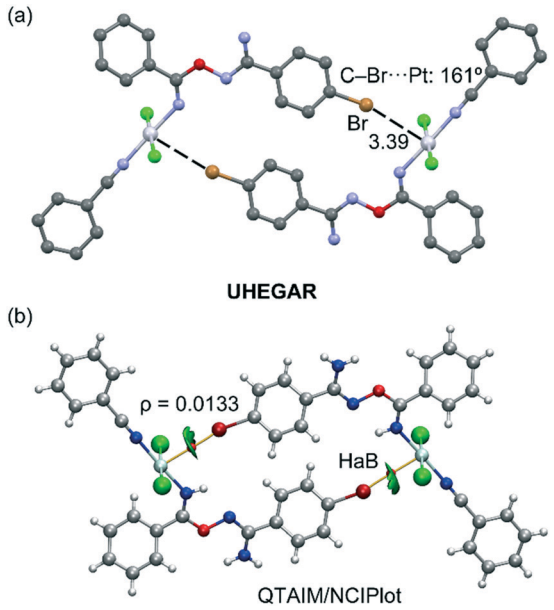

Fig. 5 (a) X-ray structure of CSD reference code **UHEGAR**. The distance is in Å. H-atoms were omitted for clarity. (b) Combined QTAIM/NCIplot analysis of **RAPQOQ** with indication of the HaB contacts. The density at the bond CP is given in a.u.

MEP surface study

The MEP surface analysis of the model compounds **1–6** (see Scheme 2) was carried out in order to study the electrophilic character of the haloarenes **1–3** and the nucleophilic character of the square planar complexes **4–6**. The surfaces are presented in Fig. 6, showing as expected a σ-hole on the extension of the C–Ha bond in compounds **1–3**. The MEP value at the σ-hole increases on going from Cl to I, as expected. Moreover, the size of the σ-hole also increases going down in the group. Fig. 6a also shows the half-angles of the σ-hole cones in compounds **1–3**, which are 60° for Cl, 68° for Br, and 74° for I. It is worth mentioning that the maximum deviation from linearity in the C–Ha···M(II) contacts observed in the X-ray structures of Fig. 2–4 is 28°, thus suggesting that in all cases the positive part of the halogen atom is pointing to the metal center.

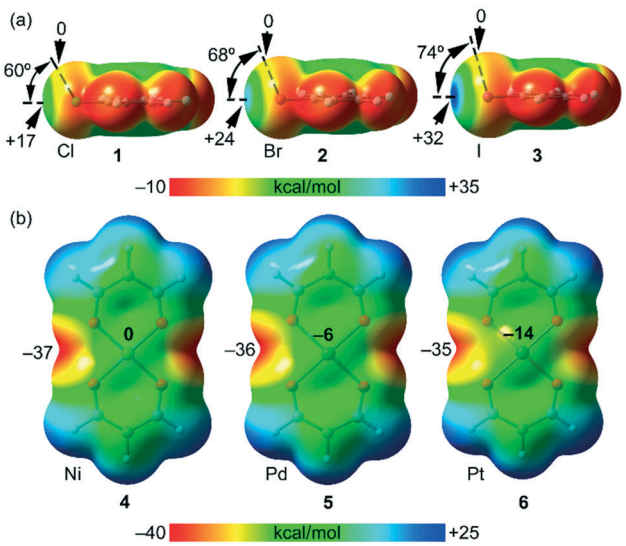

Fig. 6 MEP surfaces of σ-hole donors **1–3** (a) and acceptors **4–6** (b) at the PBE0-D3/def2-TZVP level of theory. The values at selected points of the surfaces are given in kcal mol^{-1}. Isovalue: 0.001 a.u.

Table 2 Interaction energies (E, kcal mol^{-1}), equilibrium distances (d, Å), and electron densities at the bond critical point that connects Ha with M (ρ, a.u.) for complexes **7–15** at the PBE0-D3/def2-TZVP level of theory

Complex	E	d	ρ
7 (Cl···Ni)	−2.50	3.383	0.00643
8 (Br···Ni)	−2.99	3.326	0.00907
9 (I···Ni)	−3.87	3.303	0.01249
10 (Cl···Pd)	−3.06	3.396	0.00834
11 (Br···Pd)	−3.85	3.414	0.01003
12 (I···Pd)	−4.98	3.385	0.01386
13 (Cl···Pt)	−3.38	3.442	0.00936
14 (Br···Pt)	−4.52	3.404	0.01256
15 (I···Pt)	−6.35	3.309	0.01935

In the case of the metal complexes **4–6**, the MEP minimum is located at the molecular plane, in the region bisecting the O–M–O angle. Moreover, the MEP surfaces reveal that the nucleophilicity of the metal center increases on going from Ni to Pt. In fact, the MEP is neutral over Ni(II), −6 kcal mol^{-1} over Pd(II), and −14 kcal mol^{-1} over Pt(II). This analysis anticipates weaker interactions for Ni compared to Pd or Pt.

Energetic study

Table 2 shows the interaction energies and equilibrium distances of complexes **7–15** (see Scheme 3). The interaction energies range from weak in complex **7** (−2.50 kcal mol^{-1}) to moderately strong in complex **15** (−6.35 kcal mol^{-1}), thus confirming the attractive nature of the interaction. Remarkably, the equilibrium distances are similar to those found in the X-ray structures. For instance, for the **UHEGAR** dimer, which is only stabilized by the Br···Pt halogen bond, the HaB distance is 3.39 Å and that of complex **14** is 3.404 Å, thus strongly corroborating that the interaction observed in the solid state is not simply due to packing effects. Regarding the equilibrium distances, those of the platinum complexes are shorter than those of palladium in line with the stronger

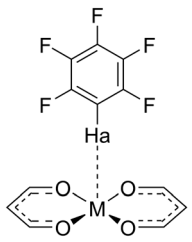

7, M = Ni, Ha = Cl
8, M = Ni, Ha = Br
9, M = Ni, Ha = I
10, M = Pd, Ha = Cl
11, M = Pd, Ha = Br
12, M = Pd, Ha = I
13, M = Pt, Ha = Cl
14, M = Pt, Ha = Br
15, M = Pt, Ha = I

Scheme 3 HaB complexes studied in this work.

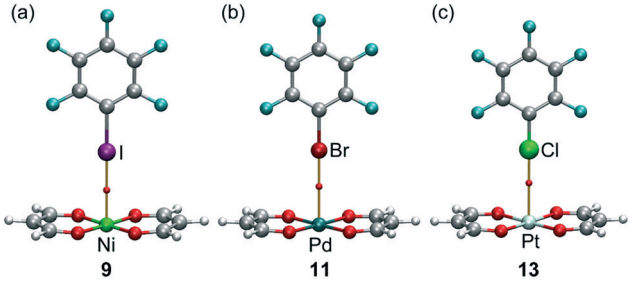

Fig. 7 QTAIM analysis of complexes **9** (a), **11** (b), and **13** (c). The bond CPs are presented as small red spheres and the bond paths are presented as orange lines. Only intermolecular interactions CPs and bond paths are presented.

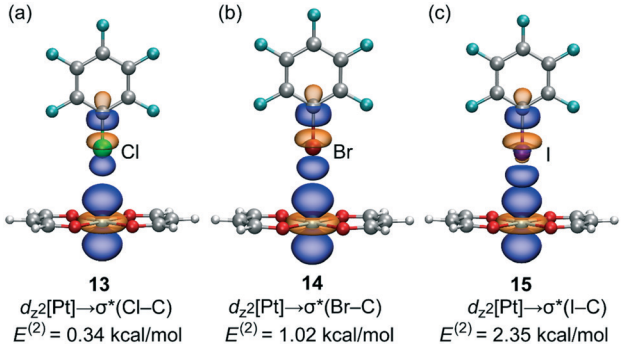

Fig. 9 Donor–acceptor NBOs characterizing HaB in complexes **13** (a), **14** (b), and **15** (c) and their second order perturbation energies ($E^{(2)}$ values). The isovalue used for the orbital representation was 0.075 a.u.

interaction energies (both metals have identical vdW radii) and the MEP results.

The geometries of three representative complexes are given in Fig. 7 along with the QTAIM analysis. It can be observed that in all cases a single bond CP connects the metal center to the halogen atom. The values of density at the bond CPs are also summarized in Table 2. For all the complexes the values of ρ are small (<0.02 a.u.) as usual in noncovalent interactions. Moreover, the values are larger for the iodine complexes in line with the shorter equilibrium distances and greater binding energies. The density values for the Br⋯Pd and Br⋯Pt complexes **11** and **14** are similar to those observed in the X-ray structures **RAPQOQ** and **UHEGAR** (see Fig. 3 and 5) which also supports the relevance of such HaB contacts in the solid state.

The values of charge density at the bond CPs have been used before as a measure of the strength of σ-hole interactions like tetrel, chalcogen, halogen, and regium bonds.[46] This behaviour was studied for HaB complexes **7**–**15** used in this work. Remarkably, a good linear relationship (regression coefficient r = 0.979) was obtained for the interaction energies *versus* ρ values plot (see Fig. 8), thus revealing that the charge density at the bond CP can also be used as a measure of the strength of HaB interactions involving metals. The importance of such relationships should be emphasized, since three different metals and halogen atoms are used, thus allowing elements from rows 3 to 6 of the periodic table to be dealt with in the same representation.

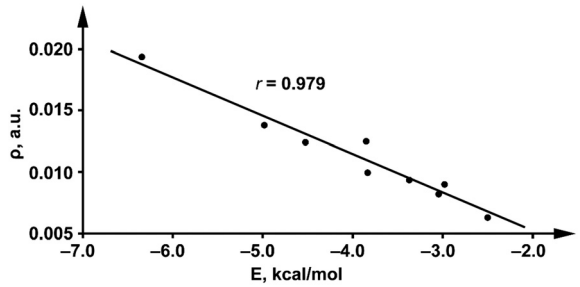

Fig. 8 Regression plot of the interaction energy *vs.* ρ at the bond CPs.

Orbital analysis

In conventional halogen bonding complexes, there is an important orbital contribution from a filled lone pair (LP) orbital to the empty antibonding Ha–Y σ* orbital stabilizing the HaB assembly.

For the Pt(II) series of complexes used in this work, natural bond orbital (NBO) analysis was performed,[47] since it is very useful to analyze donor–acceptor interactions from an orbital point of view. The results are shown in Fig. 9, clearly evidencing a d_{z^2}[Pt] → σ*(Ha–C) donor–acceptor interaction in the three complexes with concomitant second order stabilization energies ranging from $E^{(2)}$ = 0.34 kcal mol^{-1} in **13** to $E^{(2)}$ = 2.35 kcal mol^{-1} in **15**. It can be observed that the size of the σ* orbital is larger for the C–I bond than for C–Br and C–Cl, thus allowing a better overlap with the d_{z^2}[Pt] orbital, resulting in larger $E^{(2)}$ energies.

Conclusions

In this manuscript, metal-involving HaB was analysed in terms of structures retrieved from the CSD and theoretical calculations in some model systems. Although these interactions are known and they have been recently reviewed,[22] a comprehensive theoretical analysis using optimized geometries instead of crystallographic ones was not available. The relevant conclusions derived from this work are as follows: (1) HaBs involving metals are less directional than conventional HaBs; (2) the nucleophilicity of the metal increases when descending in the group; (3) the interaction energies range from −2.5 to −6.5 kcal mol^{-1}, similar to hydrogen bonds; (4) the density at the bond critical point can be used as a measure of the strength of the HaB; and, (5) a relevant orbital contribution (37%) is demonstrated for the most nucleophilic Pt metal with iodopentafluoroenzene, where the d_{z^2} orbital is acting as a LP donor.

It is expected that these counterintuitive interactions will be progressively exploited and this work could stimulate researchers working in crystal engineering, supramolecular chemistry, and catalysis to utilize metal-involving HaBs or similar interactions.

Author contributions

I. B. and R. M. G. carried out the theoretical calculations. R. M. G. computed and presented the QTAIM and NBO analyses. A. F. searched the CSD. A. F. conceived the research and wrote the manuscript. All the authors revised the original draft and contributed to the final version of the manuscript.

Conflicts of interest

There are no conflicts to declare.

Acknowledgements

We thank the MICIU/AEI of Spain (project PID2020-115637GB-I00 FEDER funds) for financial support. We thank the CTI (UIB) for the computational facilities.

Notes and references

1 G. Desiraju, *J. Am. Chem. Soc.*, 2013, **135**, 9952–9967.
2 G. Desiraju, *Angew. Chem., Int. Ed.*, 2007, **46**, 8342–8356.
3 J. S. Murray, P. Lane and P. Politzer, *J. Mol. Model.*, 2009, **15**, 723–729.
4 A. Bauzá, T. J. Mooibroek and A. Frontera, *ChemPhysChem*, 2015, **16**, 2496–2517.
5 (*a*) A. Bauzá, T. J. Mooibroek and A. Frontera, *Angew. Chem., Int. Ed.*, 2013, **52**, 12317–12321; (*b*) A. Bauzá, T. J. Mooibroek and A. Frontera, *Chem. Rec.*, 2016, **16**, 473–487.
6 S. Scheiner, *Acc. Chem. Res.*, 2013, **46**, 280–288.
7 P. Scilabra, G. Terraneo and G. Resnati, *Acc. Chem. Res.*, 2019, **52**, 1313–1324.
8 G. Cavallo, P. Metrangolo, R. Milani, T. Pilati, A. Priimagi, G. Resnati and G. Terraneo, *Chem. Rev.*, 2016, **116**, 2478–2601.
9 I. Alkorta, J. Elguero and A. Frontera, *Crystals*, 2020, **10**, 180.
10 (*a*) P. Metrangolo, H. Neukirch, T. Pilati and G. Resnati, *Acc. Chem. Res.*, 2005, **38**, 386–395; (*b*) P. Metrangolo, F. Meyer, T. Pilati, G. Resnati and G. Terraneo, *Angew. Chem., Int. Ed.*, 2008, **47**, 6114–6127; (*c*) E. Corradi, S. V. Meille, M. T. Messina, P. Metrangolo and G. Resnati, *Angew. Chem., Int. Ed.*, 2000, **39**, 1782–1786.
11 (*a*) M. Erdélyi, *Chem. Soc. Rev.*, 2012, **41**, 3547–3557; (*b*) T. M. Beale, M. G. Chudzinski, M. G. Sarwar and M. S. Taylor, *Chem. Soc. Rev.*, 2013, **42**, 1667–1680; (*c*) L. C. Gilday, S. W. Robinson, T. A. Barendt, M. J. Langton, B. R. Mullaney and P. D. Beer, *Chem. Rev.*, 2015, **115**, 7118–7195; (*d*) A. Mukherjee, S. Tothadi and G. R. Desiraju, *Acc. Chem. Res.*, 2014, **47**, 2514–2524.
12 G. Cavallo, P. Metrangolo, T. Pilati, G. Resnati and G. Terraneo, *Cryst. Growth Des.*, 2014, **14**, 2697–2702.
13 H. Hariharan, *Cryst. Growth Des.*, 2022, **22**, 2046–2049.
14 S. Portela, J. J. Cabrera-Trujillo and I. Fernández, *J. Org. Chem.*, 2021, **86**, 5317–5326.
15 (*a*) A. Frontera and A. Bauzá, *Org. Biomol. Chem.*, 2021, **19**, 6858–6864; (*b*) M. N. Piña, A. Frontera and A. Bauzá, *ACS Chem. Biol.*, 2020, **15**, 1942–1948; (*c*) A. Frontera and A. Bauzá, *J. Chem. Theory Comput.*, 2020, **16**, 4744–4752.
16 J. Pancholi and P. D. Beer, *Coord. Chem. Rev.*, 2020, **416**, 213281.
17 A. Vargas Jentzsch, D. Emery, J. Mareda, S. K. Nayak, P. Metrangolo, G. Resnati, N. Sakai and S. Matile, *Nat. Commun.*, 2012, **3**, 905.
18 (*a*) M. D. Prasanna and T. N. G. Row, *Cryst. Eng.*, 2000, **3**, 135–154; (*b*) D. Mitra, N. Bankoti, D. Michael, K. Sekar and T. N. Guru Row, *J. Chem. Sci.*, 2020, **132**, 93.
19 (*a*) X. Yu, H. Zhu and Y. Zeng, *Int. J. Quantum Chem.*, 2016, **116**, 1244–1253; (*b*) A. Bauzá and A. Frontera, *Theor. Chem. Acc.*, 2017, **136**, 1–8.
20 E. A. Katlenok, M. Haukka, O. V. Levin, A. Frontera and V. Y. Kukushkin, *Chem. – Eur. J.*, 2020, **26**, 7692–7701.
21 Z. M. Bikbaeva, D. M. Ivanov, A. S. Novikov, I. V. Ananyev, N. A. Bokach and V. Y. Kukushkin, *Inorg. Chem.*, 2017, **56**, 13562–13578.
22 D. M. Ivanov, N. A. Bokach, V. Y. Kukushkin and A. Frontera, *Chem. – Eur. J.*, 2022, **28**, e202103173.
23 A. A. Eliseeva, D. M. Ivanov, A. V. Rozhkov, I. V. Ananyev, A. Frontera and V. Y. Kukushkin, *JACS Au*, 2021, **1**, 354–361.
24 U. Dabranskaya, D. M. Ivanov, A. S. Novikov, Y. V. Matveychuk, N. A. Bokach and V. Y. Kukushkin, *Cryst. Growth Des.*, 2019, **19**, 1364–1376.
25 M. J. Frisch, G. W. Trucks, H. B. Schlegel, G. E. Scuseria, M. A. Robb, J. R. Cheeseman, G. Scalmani, V. Barone, G. A. Petersson, H. Nakatsuji, X. Li, M. Caricato, A. V. Marenich, J. Bloino, B. G. Janesko, R. Gomperts, B. Mennucci, H. P. Hratchian, J. V. Ortiz, A. F. Izmaylov, J. L. Sonnenberg, D. Williams-Young, F. Ding, F. Lipparini, F. Egidi, J. Goings, B. Peng, A. Petrone, T. Henderson, D. Ranasinghe, V. G. Zakrzewski, J. Gao, N. Rega, G. Zheng, W. Liang, M. Hada, M. Ehara, K. Toyota, R. Fukuda, J. Hasegawa, M. Ishida, T. Nakajima, Y. Honda, O. Kitao, H. Nakai, T. Vreven, K. Throssell, J. A. Montgomery Jr. , J. E. Peralta, F. Ogliaro, M. J. Bearpark, J. J. Heyd, E. N. Brothers, K. N. Kudin, V. N. Staroverov, T. A. Keith, R. Kobayashi, J. Normand, K. Raghavachari, A. P. Rendell, J. C. Burant, S. S. Iyengar, J. Tomasi, M. Cossi, J. M. Millam, M. Klene, C. Adamo, R. Cammi, J. W. Ochterski, R. L. Martin, K. Morokuma, O. Farkas, J. B. Foresman and D. J. Fox, *Gaussian 16, Revision C.01*, Gaussian, Inc., Wallingford CT, 2016.
26 S. Grimme, J. Antony, S. Ehrlich and H. Krieg, *J. Chem. Phys.*, 2010, **132**, 154104.
27 F. Weigend, *Phys. Chem. Chem. Phys.*, 2006, **8**, 1057–1065.
28 F. Weigend and R. Ahlrichs, *Phys. Chem. Chem. Phys.*, 2007, **7**, 3297–3305.
29 R. F. W. Bader, *J. Phys. Chem. A*, 1998, **102**, 7314–7323.
30 T. Lu and F. Chen, *J. Comput. Chem.*, 2012, **33**, 580–592.
31 J. Contreras-García, E. R. Johnson, S. Keinan, R. Chaudret, J.-P. Piquemal, D. N. Beratan and W. Yang, *J. Chem. Theory Comput.*, 2011, **7**, 625–632.
32 E. R. Johnson, S. Keinan, P. Mori-Sánchez, J. Contreras-García, A. J. Cohen and W. Yang, *J. Am. Chem. Soc.*, 2010, **132**, 6498–6506.
33 W. Humphrey, A. Dalke and K. Schulten, *J. Mol. Graphics*, 1996, **14**, 33–38.

34 E. D. Glendening, J. K. Badenhoop, A. E. Reed, J. E. Carpenter, J. A. Bohmann, C. M. Morales, P. Karafiloglou, C. R. Landis and F. Weinhold, *NBO 7.0*, Theoretical Chemistry Institute, University of Wisconsin, Madison, 2018.

35 (*a*) A. Bondi, *J. Phys. Chem.*, 1966, **70**, 3006–3007; (*b*) A. Bondi, *J. Phys. Chem.*, 1964, **68**, 441–451.

36 (*a*) S. S. Batsanov, *Inorg. Mater.*, 2001, **37**, 871–885; (*b*) S.-Z. Hu, Z.-H. Zhou and B. E. Robertson, *Z. Kristallogr.*, 2009, **224**, 375–383; (*c*) S. Alvarez, *Dalton Trans.*, 2013, **42**, 8617–8636.

37 B. Cordero, V. Gómez, A. E. Platero-Prats, M. Revés, J. Echeverría, E. Cremades, F. Barragán and S. Alvarez, *Dalton Trans.*, 2008, 2832–2838.

38 B. J. C. Vieira, J. C. Dias, I. C. Santos, L. C. J. Pereira, V. da Gama and J. C. Waerenborgh, *Inorg. Chem.*, 2015, **54**, 1354–1362.

39 M. Nath, J. C. Huffman and J. M. Zaleski, *J. Am. Chem. Soc.*, 2003, **125**, 11484–11485.

40 Y. Wang, N. Okabe and M. Odoko, *Chem. Pharm. Bull.*, 2005, **53**, 1291–1295.

41 M. A. Taige, A. Zeller, S. Ahrens, S. Goutal, E. Herdtweck and T. Strassner, *J. Organomet. Chem.*, 2007, **692**, 1519–1529.

42 J. L. Serrano, L. García, J. Pérez, E. Pérez, J. García, G. Sánchez, P. Sehnal, S. de Ornellas, T. J. Williams and I. J. S. Fairlamb, *Organometallics*, 2011, **30**, 5095–5109.

43 D. M. Ivanov, A. S. Novikov, I. V. Ananyev, Y. V. Kirina and V. Yu. Kukushkin, *Chem. Commun.*, 2016, **52**, 5565–5568.

44 A. V. Rozhkov, D. M. Ivanov, A. S. Novikov, I. V. A. Nadezhda, A. Bokach and V. Yu. Kukushkin, *CrystEngComm*, 2020, **22**, 554–563.

45 D. S. Bolotin, M. Ya. Demakova, A. S. Novikov, M. S. Avdontceva, M. L. Kuznetsov, N. A. Bokach and V. Yu. Kukushkin, *Inorg. Chem.*, 2015, **54**, 4039–4046.

46 (*a*) M. Michalski, A. J. Gordon and S. Berski, *Polyhedron*, 2021, **210**, 115495; (*b*) A. Bauza, D. Quiñonero, A. Frontera and P. M. Deya, *Phys. Chem. Chem. Phys.*, 2011, **13**, 20371–20379; (*c*) A. Franconetti and A. Frontera, *Dalton Trans.*, 2019, **48**, 11208–11216; (*d*) S. Grabowski, *J. Phys. Chem. A*, 2012, **116**, 1838–1845; (*e*) B. Galmés, J. Adrover, G. Terraneo, A. Frontera and G. Resnati, *Phys. Chem. Chem. Phys.*, 2020, **22**, 12757–12765; (*f*) M. N. Piña, S. Burguera, J. Buils, M. A. Crespí, J. Ernesto Morales, J. Pons, A. Bauzá and A. Frontera, *ChemPhysChem*, 2022, **23**, e202200010.

47 E. D. Glendening, C. R. Landis and F. Weinhold, *J. Comput. Chem.*, 2019, **40**, 2234–2241.

